Earth and Planetary Science Letters 533 (2020) 116057

Contents lists available at ScienceDirect

Earth and Planetary Science Letters

www.elsevier.com/locate/epsl

Ferromanganese crusts as recorders of marine dissolved oxygen

Kevin M. Sutherland [a,b], Jordan A.G. Wostbrock [c], Colleen M. Hansel [a], Zachary D. Sharp [c], James R. Hein [d], Scott D. Wankel [a,*]

[a] Department of Marine Chemistry and Geochemistry, Woods Hole Oceanographic Institution, 266 Woods Hole Road, Woods Hole, MA 02543, USA
[b] Department of Earth, Atmospheric and Planetary Sciences, Massachusetts Institute of Technology, 77 Massachusetts Avenue, Cambridge, MA 02139, USA
[c] Department of Earth and Planetary Sciences, University of New Mexico, Albuquerque, NM 87131, USA
[d] Pacific Coastal and Marine Science Center, US Geological Survey, 2885 Mission St., Santa Cruz, CA 95060, USA

ARTICLE INFO

Article history:
Received 27 June 2019
Received in revised form 28 December 2019
Accepted 29 December 2019
Available online xxxx
Editor: L. Robinson

Keywords:
ferromanganese crust
triple oxygen isotopes
marine dissolved oxygen

ABSTRACT

The distinct triple oxygen isotope composition of tropospheric O_2 relative to seawater is the result of biogeochemical reactions (e.g. primary productivity, respiration), exchange with the stratosphere, and the relative size of different oxygen-containing reservoirs, namely O_2, O_3, and CO_2. This difference in isotopic composition gives tropospheric O_2 utility as a record of biogeochemical and atmospheric processes and may also be used for determining where in the rock record isotopic fingerprints of tropospheric oxygen may be preserved. The isotopic record of tropospheric oxygen in previous studies is largely limited to analyses of gas trapped in continental glaciers and a patchwork of other proxies, most notably the triple oxygen signature of sulfate. Here we show the uppermost layers of hydrogenetic, deep-ocean ferromanganese crusts from each of the major ocean basins have a triple oxygen isotope composition consistent with the direct incorporation of dissolved oxygen. The range of $\delta^{18}O$ and $\Delta'^{17}O$ in ferromanganese crusts suggests the Mn oxide endmember contains a near 50:50 mixture of oxygen from water and dissolved O_2. Our data indicate this signal also persists into older layers of the crusts, potentially preserving near 75 million years of the oxygen isotopic composition of the lower troposphere and subsequent deep-ocean respiration. Our analysis of oxygen isotope values, bulk chemistry, and estimated local dissolved oxygen for crust top samples reveals that variations in bulk chemistry ultimately exhibit more influence on the oxygen mass balance than changes in dissolved oxygen, presenting a challenge for unambiguous determination of local dissolved oxygen. Although analytical challenges remain, these widespread, layered deposits of ferromanganese crust may offer a viable path for future interrogation of the history or relative history of the oxygen cycle of the troposphere and deep ocean millions of years into the past.

1. Introduction

The $^{18}O/^{16}O$ ratio of diatomic oxygen (expressed as $\delta^{18}O_{O2}$) in the troposphere integrates biogeochemical reactions and atmospheric exchange processes that produce, consume, and mix O_2 (Bender et al., 1994). The $\delta^{18}O_{O2}$ of the modern troposphere ($\sim +24‰$) (Barkan and Luz, 2005; Wostbrock et al., 2020) is set primarily by mass-dependent processes that discriminate against the heavier isotopes during reduction of O_2 or evapotranspiration of leaf water (e.g., the 'Dole Effect') (Bender et al., 1994; Hoffmann et al., 2004). Ice core records indicate that the $\delta^{18}O_{O2}$ of the troposphere has fluctuated by $> 1‰$ over the last hundred thousand years, primarily due to changes in the $\delta^{18}O$ of seawater from the periodic sequestration of isotopically light water in continental ice and changes in the magnitude of the Dole effect (Bender et al., 1994). In comparison, the $^{17}O/^{16}O$ composition of tropospheric O_2, typically expressed in linearized form as $\Delta'^{17}O$ ($\Delta'^{17}O = \delta'^{17}O - \lambda\delta'^{18}O$, with $\lambda = 0.528$ used in this study), is controlled by mass-dependent processes and vertical mixing with the stratosphere where mass-independent exchange reactions occur (Blunier et al., 2002; Luz et al., 1999; Thiemens and Heidenreich, 1983). The $\Delta'^{17}O$ value of tropospheric O_2 is influenced by the partial pressures of CO_2 and O_2, their biogeochemical fluxes, and atmospheric vertical exchange (Cao and Bao, 2013; Thiemens, 2006). Importantly, modern tropospheric O_2 ($\Delta'^{17}O \approx -0.5‰$) has a triple oxygen isotope signature distinct from that of ocean water ($\Delta'^{17}O = 0‰$), which can be used as an independent tracer of O_2 cycling dynamics (Barkan and Luz, 2005; Luz et al., 1999; Pack et al., 2017; Wostbrock et al., 2020).

* Corresponding author.
E-mail address: sdwankel@whoi.edu (S.D. Wankel).

https://doi.org/10.1016/j.epsl.2019.116057
0012-821X/

Table 1
Ferromanganese crust sample location.

Fig. 1 ID	Cruise ID	Sample No.	Water depth (m)	Latitude	Longitude
1	Antipode (ANTP)	109D-E-L0-12	5698-5778	−27.980	60.803
2	Antipode (ANTP)	145D-D3	2748-2094	−7.333	57.938
3	DODO	232D-B-L0-11	4119-3558	−5.383	97.483
4	F10-89-CP	D11-1K	1870-1690	11.648	161.675
5	HLY1202	DR3-035	1605	78.700	−160.050
6	HLY1202	DR3-036	1605	78.700	−160.050
7	MW-8801	D18-1F	3993	−50.040	126.742
8	PLUME 02	D3-1B	2035-1885	−1.010	−85.658
9	S6-79-NP	D4-13A	2100	53.543	−144.373
10	MBARI 2004	T667-R41A	1033.7	32.394	−120.084
11	TN037	D4-1B	4000	39.838	163.913
12	VULCAN 5 (VULC)	D34-39A	3983-3684	−57.782	−7.672
13	F7-86-HW	CD29-2B	2390-1970	16.707	−168.237

The coarse and fine details of the oxygen cycle elucidated by direct measurements of $\delta^{18}O$ and $\Delta'^{17}O$ of atmospheric O_2 are largely limited to paleo-atmosphere trapped in continental ice (Bender et al., 1994; Blunier et al., 2002). These studies have used the oxygen isotope composition of ice-trapped atmosphere to estimate primary production in marine and terrestrial environments and identify the key influences on O_2 cycling dynamics on timescales up to $\sim 100{,}000$ yr. As a high-potential oxidant of many reduced materials on the surface earth, the isotopic signature of O_2 can be retained by some oxygen-bearing minerals (e.g., sulfate (Crockford et al., 2018), phosphate (Gehler et al., 2011)), though oxygen isotope exchange of biotic or abiotic origin can confound interpretation and limit the timescales on which questions about past oxygen cycling can be addressed.

Manganese oxides are extremely common and geographically widespread in marine environments (Uramoto et al., 2019), exceeding 50% coverage of the seafloor in some abyssal regions of the global ocean (Hein and Koschinsky, 2014). Manganese(II) oxidation by O_2 can be facilitated by biological or abiotic processes, including enzyme catalysis, surface and ligand complexation, or reactive oxygen species (ROS) of various origins (Learman et al., 2011; Sutherland et al., 2018; Tebo et al., 2005). Study of synthetic manganese (Mn) oxy(hydr)oxide minerals (hereafter referred to as Mn oxides) suggests they capture and retain oxygen atoms from dissolved O_2 during oxidation of aqueous Mn(II) to insoluble Mn(III/IV) (Mandernack et al., 1995; Sutherland et al., 2018). $\Delta'^{17}O$ values of one natural ferromanganese nodule suggests the same may be true in natural Mn oxides (Sharp et al., 2018), though comprehensive confirmation that this occurs in all natural low temperature Mn oxides has not yet been achieved (Luther, 2010; Mandernack et al., 1995; Sutherland et al., 2018). Thus, Mn oxides, if resistant to isotopic exchange with ambient water, could serve as a valuable isotopic proxy for O_2 over the lifetime of the oceanic crust on which these deposits form.

Let us consider what information may be gained from a detailed geochemical proxy for the triple oxygen isotope composition of dissolved oxygen. Gas exchange at the ocean surface leads to isotopic equilibrium between the atmosphere and dissolved gases. Following deep-water formation, the primary process influencing dissolved O_2 (DO) is the reduction of O_2 by biological processes, the most consequential being respiration. The biological reduction of O_2 roughly follows a closed-system Rayleigh fractionation curve (in addition to advection and diffusion), producing a monotonic increase in $\delta^{18}O$ with decreasing concentrations of DO (Kroopnick, 1980; Levine et al., 2009; Stolper et al., 2018). The $\delta^{18}O$ of dissolved oxygen in the marine water column typically ranges from $\sim +23‰$ in productive surface waters to greater than $+40‰$ near the oxygen minimum (Levine et al., 2009). Assuming $\sim 50\%$ of oxygen atoms in the Mn-oxide endmember are from dissolved O_2, we would expect the oxygen isotope signature of Mn oxides to track

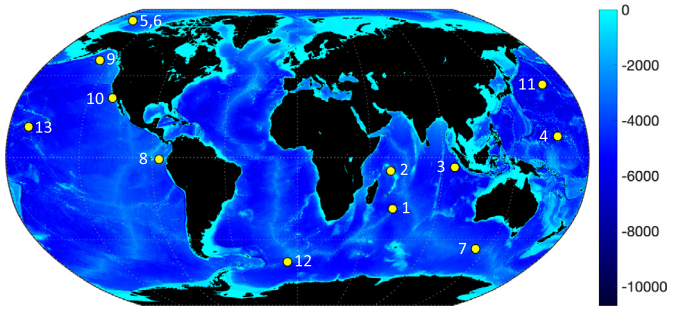

Fig. 1. Distribution of ferromanganese crusts analyzed in this study with seafloor depth given in meters.

that of O_2 with approximately half the magnitude and an offset accounting for any isotope fractionation.

Hydrogenetic, deep-ocean ferromanganese crusts have several characteristics that make them ideal hosts of such a geochemical proxy. Ferromanganese crusts are geographically widespread, form as layered deposits offering a clear sense of time, and age within a narrow temperature range. These deposits primarily constitute a co-precipitated mixture of Mn and Fe oxide phases, and often contain several weight percent of detrital or authigenic silicates and transition metals including cobalt, nickel, and copper. While the heterogeneity of ferromanganese deposits presents a challenge to isolating individual phases, here we demonstrate that bulk ferromanganese-crust compositions contain clear indication of atmospheric O_2 in deposits over 30 Ma old and assess their fidelity as an isotopic record of DO. Below we first consider the $\delta^{18}O$ of natural ferromanganese deposits in both new and historical datasets (Section 3.1), followed by new insights offered by triple oxygen isotope results for the same sample set (Section 3.2).

2. Materials and methods

2.1. Sample location and preparation

The top-most portion of each ferromanganese crust in this study served as the primary analytical target as it represents the youngest crust, and has had the least amount of time to undergo possible post-depositional alteration. The top 0.5 mm to 3 mm was sampled from each crust using a ceramic blade. Sample locations and information are presented in Table 1 and shown in Fig. 1. The geochemistry of ten major elements for the samples was determined by X-ray fluorescence (XRF) on borate fused discs, which is included in the supplementary information along with sample ID, latitude and longitude, water depth, and the crust depth interval on which XRF was collected. Due to the difference in sampling

Table 2
Triple oxygen isotope values of ferromanganese crusts.

Crust top	$\delta^{17}O$	$\delta^{18}O$	$\delta'^{17}O$	$\delta'^{18}O$	$\Delta'^{17}O$ ($\lambda = 0.528$)	$\Delta'^{17}O$ ($\lambda = 0.5305$)	$\theta_{EQ\text{-inferred}}$
ANTP 109D-E-L0-12	5.450	10.516	5.435	10.461	−0.088	−0.114	0.520
ANTP 109D-E-L0-12 (2)	4.944	9.554	4.932	9.509	−0.089	−0.113	0.519
ANTP 145D-D3	3.837	7.451	3.830	7.423	−0.089	−0.108	0.516
DODO 232D-B-L0-11	4.639	9.021	4.628	8.981	−0.114	−0.136	0.515
F10-89-CPD11-1K	4.792	9.347	4.781	9.304	−0.132	−0.155	0.514
F10-89-CPD11-1K (2)	5.296	10.273	5.282	10.221	−0.115	−0.140	0.517
HLY1202DR3-035	5.488	10.627	5.473	10.571	−0.108	−0.135	0.518
HLY1202DR3-036	5.825	11.277	5.808	11.214	−0.113	−0.141	0.518
MW-8801 D18-1F	5.456	10.562	5.441	10.507	−0.107	−0.133	0.518
MW-8801 D18-1F (2)	4.948	9.594	4.936	9.548	−0.105	−0.130	0.517
PLUME 02 D3-1B	5.415	10.523	5.400	10.468	−0.127	−0.153	0.516
PLUME 02 D3-1B (2)	4.705	9.113	4.694	9.072	−0.096	−0.119	0.517
PLUME 02 D3-1B (3)	5.564	10.843	5.549	10.785	−0.145	−0.173	0.514
S6-79-NP D4-13A	6.049	11.702	6.031	11.634	−0.112	−0.141	0.518
S6-79-NP D4-13A (2)	4.348	8.432	4.339	8.397	−0.095	−0.116	0.517
MBARI 2004T667-R41A	3.427	6.707	3.421	6.685	−0.109	−0.125	0.512
TN037D4-1B	6.167	11.945	6.148	11.874	−0.121	−0.151	0.518
VULC D34-39A	5.225	10.089	5.211	10.038	−0.089	−0.114	0.519
VULC D34-39A (2)	5.047	9.782	5.034	9.734	−0.106	−0.130	0.517
Down crust							
F7-86-HW CD29 0-2.5 mm	4.113	8.186	4.105	8.153	−0.200	−0.220	0.503
F7-86-HW CD29 7-9.5 mm	3.891	7.703	3.883	7.673	−0.168	−0.187	0.506
F7-86-HW CD29 14-16.5 mm	4.286	8.413	4.277	8.378	−0.147	−0.168	0.510
F7-86-HW CD29 14-16.5 mm (2)	4.070	8.043	4.062	8.011	−0.168	−0.188	0.507
F7-86-HW CD29 21-23.5 mm	3.535	7.002	3.529	6.978	−0.155	−0.173	0.506
F7-86-HW CD29 21-23.5 mm (2)	2.547	5.115	2.544	5.102	−0.150	−0.163	0.499
F7-86-HW CD29 28-30.5 mm	2.995	5.993	2.991	5.975	−0.164	−0.179	0.500
F7-86-HW CD29 35-37.5 mm	3.900	7.776	3.892	7.746	−0.198	−0.217	0.503
F7-86-HW CD29 35-37.5 mm (2)	3.932	7.779	3.924	7.749	−0.167	−0.187	0.506

(2) and (3) indicate duplicate and triplicate analyses, respectively.

intervals between XRF analysis and triple oxygen isotope analysis, the geochemical data presented in the supplementary information should be considered an approximation in relation to the triple oxygen isotope data. Sampling of CD29 below the stratigraphic intervals presented in Table 2 was not conducted due to significant phosphatization (formation of authigenic carbonate fluorapatite) in the crust (Frank et al., 1999). Ferromanganese crusts may also host extraterrestrial material (e.g. micrometeorites, cosmic spherules) in their matrix (Basu et al., 2006; Halbach et al., 1989). Meteorites typically exhibit anomalous $\Delta'^{17}O$ values, typically ranging from -1 to $+1$‰, with some exceptions (Clayton et al., 1983; Clayton and Mayeda, 1996). One study found such extraterrestrial material made up approximately 2 ppm of a ferromanganese crust by mass (Halbach et al., 1989). Given the low abundance of extraterrestrial material in ferromanganese crusts, we will not consider this minor contribution in subsequent oxygen isotope mass balance calculations.

2.2. Oxygen isotope measurements

Samples were analyzed using a ThermoFinnigan MAT 253 configured for O_2 analysis at the University of New Mexico Center for Stable Isotopes. All samples were analyzed as O_2 gas, which was extracted using conventional laser fluorination (Sharp, 1990). Each sample was placed in a drying oven (110 °C) for a minimum of 12 hours prior to handling to drive off adsorbed water. We measured the effect of this drying procedure on the average Mn oxidation state of one sample (CD29 0-2.5 mm, average oxidation state: +3.5) using X-ray absorption spectroscopy and found no significant change in the average Mn oxidation state before and after drying. The dried samples were weighed (2-4 mg) before introduction to the fluorination chamber. Samples were pre-fluorinated with 100 mbar BrF_5 gas for approximately 1-2 hours. Prior to the analyses presented in this study, we observed a steady decrease in sample O_2 yield and $\delta^{18}O$ value the longer a standard was exposed to BrF_5 in the sample chamber. Given the direction of the $\delta^{18}O$ shift, we concluded that one of the components in the ferromanganese material was undergoing passive reaction with BrF_5. Submerging the sample chamber in an ice bath during sample fluorination prevented this passive reaction; all analyses reported in this study were measured using this procedure. Following O_2 extraction, the sample was passed through multiple liquid nitrogen traps, a warm sodium chloride trap, and a gas chromatography column to remove contaminants. The effluent O_2 was condensed onto a 5 Å molecular sieve and the carrier gas (ultra-high purity helium) was pumped away prior to introduction into the mass spectrometer. The reference gas used in this study is calibrated to VSMOW and SLAP, and all values are standardized to the VSMOW-SLAP scale. The delta values presented in this study ($\delta^{x}O = ({}^{x}R_{sample}/{}^{x}R_{standard} - 1) \times 1000$, ${}^{x}R_{sample} = {}^{x}O/{}^{16}O$) are converted to linearized delta notation ($\delta'^{x}O = 1000(\ln(1+\delta^{x}O/1000))$) (Hulston and Thode, 1965; Miller, 2002). The oxygen-17 compositions are reported using the $\Delta'^{17}O$ value, defined as $\Delta'^{17}O = \delta'^{17}O - \lambda\delta'^{18}O$, where λ is a reference slope. We use $\lambda = 0.528$ to report values in this study's text, table, and figures, and include $\Delta'^{17}O$ values calculated using $\lambda = 0.5305$ (theoretical high temperature limit) for ease of comparison to studies using this convention. We also discuss θ values of equilibrium and kinetic processes throughout the text, which are defined as $\theta = \ln{}^{17}\alpha / \ln{}^{18}\alpha$, ${}^{x}\alpha = {}^{x}R_A/{}^{x}R_B$, respectively, where A and B represent two oxygen-bearing compounds.

There has been only limited investigation on the triple oxygen isotopic analysis of ferromanganese materials. The $\delta^{18}O$ values of some Mn oxides and ferromanganese materials have been previously measured (Mandernack et al., 1995; Sutherland et al., 2018; Yeh et al., 1985). We performed an interlaboratory comparison of $\delta^{18}O$ of a widely available ferromanganese reference material (USGS Nod-A-1) to ensure that the oxygen isotope measurements are robust and sample conversions to O_2 were near complete. Bulk and trace metal chemistry for USGS Nod-A-1 have

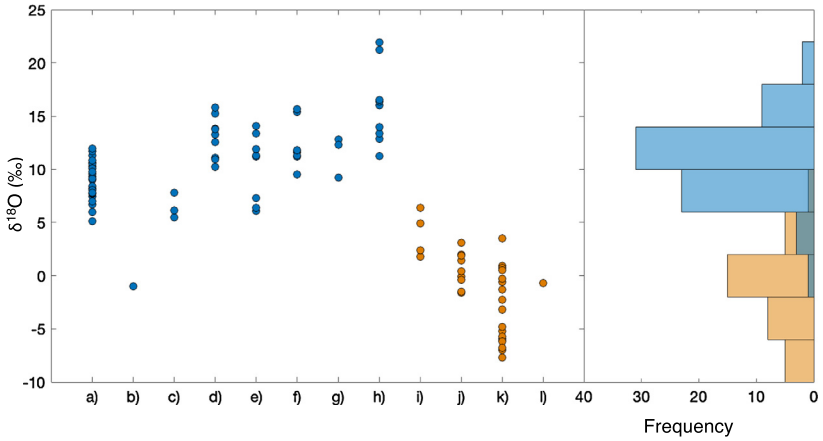

Fig. 2. $\delta^{18}O$ of manganate samples (left) and frequency distribution of marine and non-marine manganate $\delta^{18}O$ values. Marine samples (blue) are separated by study and sample type. Marine samples from left to right are a) ferromanganese crusts in this study, b) hydrothermal manganate lens from Franciscan assemblage (Chyi et al., 1984), c) hydrothermal manganate from Kaikata seamount (Mandernack et al., 1995), d) Pacific ferromanganese nodules (Dymond et al., 1973), e) ferromanganese crusts and nodules (Yeh et al., 1985), f) ferromanganese nodule near Hawaii (Sharp et al., 2018), g) ferromanganese nodules from Blake Plateau (Bar-Matthews and Matthews, 1990), and h) Mn and Fe oxide-rich sediment (Dymond et al., 1973). Non-marine samples (orange) from left to right are i) a freshwater ferromanganese nodule (Mandernack et al., 1995), j) endmember sedimentary Mn oxides (Bar-Matthews and Matthews, 1990), k) volcanogenic and sedimentary Mn oxides (Yeh et al., 1985), and l) manganese oxide from Hotazel Formation (Levin et al., 2014).

been previously characterized (Flanagan and Gottfried, 1980). For inter-laboratory comparison, USGS Nod-A-1 was measured on the MAT 253 at UNM and also at the Woods Hole Oceanographic Institution (WHOI) using high temperature micro-fluorination on an Isoprime100 IRMS (analytical precision ±0.4‰ for Mn oxides). In short, samples run with micro-fluorination method were packed with Teflon powder and pyrolyzed at 1450 °C. A more detailed treatment of the method is described elsewhere (Menicucci et al., 2013; Sutherland et al., 2018). The mean $\delta'^{18}O$ of USGS Nod-A-1 was $+11.600 \pm 1.544$‰ (n=9) and $+11.8 \pm 0.7$‰ (n=9) measured at UNM and WHOI, respectively. No statistically significant difference was observed between the two sets of measurements (two-sample t-test, p=0.73). $\Delta'^{17}O$ values could only be measured using the conventional fluorination method. The $\Delta'^{17}O$ value of Nod-A-1 is -0.112 ± 0.014 (n=9).

2.3. Estimate of marine dissolved oxygen

Measurements of marine dissolved O_2 are routinely collected as a part of oceanographic research, making a direct comparison between the oxygen isotope composition of ferromanganese crust and an estimate of local DO concentration possible. The World Ocean Atlas 2018 (WOA2018) offers sufficient spatial resolution to produce such an estimate for each of the sample locations in this study (Garcia et al., 2018). The WOA2018 dissolved oxygen data was queried for the dissolved oxygen concentration at the latitude, longitude, and depth closest to the sample location (data shown in Table S1). If the sample depth was not available at the closest latitude and longitude, the next closest cell for which the sample depth was available was used. We also manually inspected adjacent data points to ensure dissolved oxygen concentrations smoothly varied locally.

3. Results and discussion

3.1. $\delta^{18}O$ of manganese oxides

We determined the $\delta^{18}O$ values of 13 ferromanganese crusts from 12 locations throughout the global ocean (Fig. 1). The range of $\delta^{18}O$ values of these ferromanganese crusts spans from +5.1‰ to +11.9‰ (average: +9.0, standard deviation: 1.7‰), with top-layer samples occupying a slightly more limited range (+6.7‰ to +11.9‰, average: +9.7‰, standard deviation: 1.3‰, Table 2). The stratigraphically older subsamples of F7-86-HW CD29 ranged from +5.1‰ to +8.4‰ (average: +7.2‰, standard deviation: 1.1‰). The range of $\delta^{18}O$ values in the sample set may reflect a variety of factors, including different environmental conditions (e.g. O_2 concentration), bulk chemistry and/or mineralogy, or diagenesis. The $\delta^{18}O$ values alone cannot be used to distinguish these processes because the oxygen isotope mass balance is underconstrained when the isotopic composition of water or O_2 is unknown *a priori*. In addition to multiple oxygen sources, variability among isotope fractionation factors, the relative contribution of each oxygen source, Mn oxidation state, and the partial or complete isotopic equilibration with ambient water may confound the $\delta^{18}O$ values of natural manganates. To determine what information can be gathered from $\delta^{18}O$ values, we compiled every oxygen isotope measurement of Mn oxides and Mn oxide-rich material available in the literature (103 measurements; Fig. 2) (Bar-Matthews and Matthews, 1990; Chyi et al., 1984; Dymond et al., 1973; Levin et al., 2014; Mandernack et al., 1995; Sharp et al., 2018; Yeh et al., 1985). We categorize previous samples as either non-marine, which range from −7.7‰ to +6.4‰, or marine samples, which range from −1.0‰ to +21.9‰. If we omit marine samples exhibiting clear evidence of hydrothermal alteration and those containing a significant portion of silicate material, the range of $\delta^{18}O$ of marine Mn oxides narrows to +5.5‰ to +15.8‰. This range is more than double that of deep ocean marine carbonates over the last 70 Myr (e.g. Zachos et al., 2001).

A bimodal separation is evident, where non-marine Mn oxides have a lower $\delta^{18}O$ value than marine Mn oxides ($p < 0.0001$, two-sample t-test) (Fig. 2). Non-marine samples average −1.4‰, while marine samples average +10.8‰. The difference between the average marine and non-marine samples, ∼ 12 per mil, bears the oxygen isotope fingerprints of ocean and meteoric water. However, such an interpretation is complicated by complex thermal histories, incomplete mineralogical information, unknown source oxygen, and compositional heterogeneity. In fact, an outlier among the marine samples, a hydrothermal Mn oxide lens from the Franciscan Assemblage, has a calculated $\delta^{18}O$ value of −1.0‰ for the Mn oxide and reflects a clear history of hydrothermal alteration in the presence of seawater (Chyi et al., 1984). The differences between terrestrial vs. marine Mn oxides and primary vs. hydrothermal marine Mn oxides could be reconciled by one or more of three likely

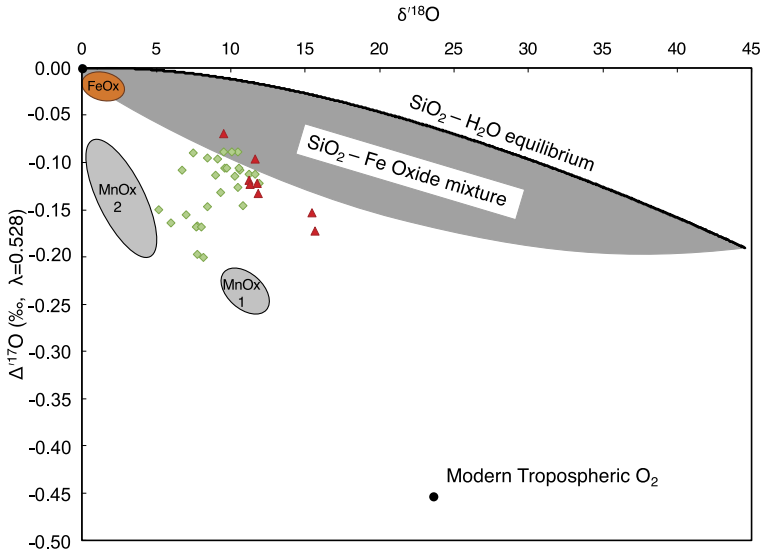

Fig. 3. Triple oxygen isotope values of marine ferromanganese crusts from this study (green) and a ferromanganese nodule from near Hawaii (Sharp et al., 2018) (red). The triple oxygen isotope composition of seawater ($\delta'^{18}O = 0$ and $\Delta'^{17}O = 0$) and tropospheric oxygen ($\delta'^{18}O = +23.6‰$ and $\Delta'^{17}O = -0.452‰$) are plotted. The theoretic triple oxygen isotope range of low-temperature Fe oxides (Hayles et al., 2018) (orange circle), detrital and authigenic silicates (SiO_2-H_2O equilibrium line (Sharp et al., 2016), solid black curve), and the range of mixtures between these two components (gray lined area) is unable to explain the distribution of $\delta'^{18}O$ and $\Delta'^{17}O$ of ferromanganese crusts. The Mn oxide endmember requires a lower $\Delta'^{17}O$ to satisfy the three-component mass balance. We include two candidate Mn-oxide endmembers. MnOx1 represents a theoretical Mn-oxide endmember with 40-60% mixture of dissolved oxygen and seawater oxygen without significant fractionation (Mandernack et al., 1995). MnOx2 is the theoretical Mn oxide endmember assuming a 40 to 60% mixture of dissolved oxygen and seawater oxygen (Sutherland et al., 2018), a large oxygen isotope effect (−17 to −23‰ (Sutherland et al., 2018)), and a typical kinetic mass relationship of $\theta_{KIE} = 0.515$-0.520.

scenarios. First, all Mn oxides could be in oxygen isotope equilibrium with its water of formation (marine or meteoric), with higher $\delta^{18}O$ values corresponding to lower water temperatures. Second, mineralogical differences (e.g. Mn oxide mineral phases) may produce different equilibrium oxygen fractionation factors between water and Mn oxide minerals. Lastly, low-temperature Mn oxides (which may or may not derive their oxygen from O_2) may not typically exchange oxygen with the surrounding water except when exposed to high temperatures or certain recrystallization conditions, causing oxygen atoms to re-equilibrate with ambient water.

One anecdotal comparison between marine Mn oxides and a freshwater Mn oxide formed in water of known $\delta^{18}O$ composition provides a useful perspective for narrowing down the most parsimonious model for oxygen isotope systematics in our data compilation. A freshwater ferromanganese nodule from Lake Oneida ($\delta^{18}O_{H2O} = -8.9‰$) has a calculated Mn-oxide $\delta^{18}O$ value of +7.5‰, 16.4‰ higher than the corresponding lake water (Mandernack et al., 1995). By comparison, the average marine Mn oxide has a $\delta^{18}O$ value of +10.8‰, corresponding to an offset of +10.8‰ from the $\delta^{18}O$ value of seawater (∼ 0‰). Thus, the difference between the $\delta^{18}O$ values of marine and freshwater Mn oxides (3.3‰) is only ∼ 40% the difference between the $\delta^{18}O$ values of their waters of formation (8.9‰). This difference is unlikely to be explained only by temperature since the approximate temperature difference is just a few degrees C (Mandernack et al., 1995). The lack of 1:1 correlation between the $\delta^{18}O$ values of Mn oxides and their environmental water is consistent with the incorporation of DO in hydrogenetic Mn oxides, and is explained by a ∼ 60% contribution from dissolved O_2. The 40% incorporation of oxygen atoms from ambient water with the remainder coming from DO is supported by controlled laboratory experiments that found 38%–62% O_2 incorporation among several biotic and abiotic Mn oxidation reactions (Mandernack et al., 1995; Sutherland et al., 2018). Although this single freshwater oxide is consistent with the oxygen isotope framework presented in previous studies, we caution the reader that more measurements of freshwater systems are necessary for a robust comparison.

3.2. $\Delta'^{17}O$ of manganese oxides

Triple oxygen isotope measurements provide an additional dimension to explore the oxygen source to ferromanganese crusts. The $\Delta'^{17}O$ values of ferromanganese crusts in this global crust-top survey ranged from −0.088‰ to −0.200‰ (Table 2). Measured values in the stratigraphic study of CD29 ranged from −0.147‰ to −0.200‰. The only other reported values of $\Delta'^{17}O$ for marine ferromanganese deposits similarly range from −0.070‰ to −0.172‰ (Sharp et al., 2018). Intriguingly, these Mn oxides occupy a unique region in oxygen three-isotope space that is not shared by any commonly measured Earth materials (Fig. 3) and are inferred to have incorporated low-$\Delta'^{17}O$ from dissolved diatomic oxygen (Mandernack et al., 1995; Sharp et al., 2018; Sutherland et al., 2018). We can better contextualize the distribution of ferromanganese triple oxygen isotope compositions by considering their bulk chemistry. The primary oxygen-bearing phases in ferromanganese crusts include Mn and Fe oxides, with minor contributions from silicate phases (bulk ferromanganese crust chemistry data provided in the SI). While other metal oxides are present, some of which may share oxygen bonds with the primary Mn, Fe, or Si phases, their contributions to the oxygen mass balance is minor and we do not consider them here. Of these three primary oxygen-bearing mineral groups, the systematic experimental or theoretical investigation of mineral-water triple oxygen isotope equilibria have only been conducted for a few iron (Fe) oxide and silicate minerals (Hayles et al., 2018; Sharp et al., 2016). Authigenic Fe oxides (hematite and magnetite) formed at bottom water temperatures are expected to have a $\Delta'^{17}O$ value no lower than −0.040‰ ($\delta'^{18}O = \sim 3‰$ at 0 °C) (Hayles et al., 2018). Iron oxides in ferromanganese crusts are typically poorly crystalline Fe oxyhydroxides having a presumably similar $\Delta'^{17}O$ values to other Fe oxides and thus to that of seawater (Frank et al., 1999; Hein and Koschinsky, 2014). In comparison, silicates of detrital or authigenic origin may span a much wider range of $\Delta'^{17}O$ values (Sharp et al., 2016). The $\Delta'^{17}O$ values of detrital silicates from high temperature systems are approximately 0‰, while low-temperature silica deposits (e.g. chert or opal) formed in 0 °C seawater will have $\delta'^{18}O$ and

$\Delta'^{17}O$ values of +44.5‰ and −0.190‰, respectively. The triple oxygen isotope values of other silicate minerals will likely vary from the pure SiO_2–water equilibrium isotope fractionation curve, though a systematic analysis of other relevant silicates has not been conducted. One anecdotal data point of a clay mineral, which are commonly present in ferromanganese crusts, falls very close to the SiO_2-H_2O equilibrium line (e.g. kaolinite $\delta'^{18}O = 24.536$‰ and $\Delta'^{17}O = -0.030$‰) (Sengupta, 2016) (Fig. 3). For simplicity, we assume any silicates present in the crust fall on this SiO_2-H_2O equilibrium line. The range of $\delta'^{18}O$ and $\Delta'^{17}O$ values from a mixture of silicate and low-temperature Fe oxides cannot produce a $\Delta'^{17}O$ low enough to describe the bulk ferromanganese crust values (Fig. 3). In sum, the Mn-oxide endmember must have lower $\Delta'^{17}O$ values to explain the bulk crust values.

For completeness, we consider three plausible explanations for the distribution of $\delta'^{18}O$ and $\Delta'^{17}O$ in Mn-oxide minerals. First, ferromanganese crusts may reflect mineral-water oxygen isotope equilibrium between oxide and seawater. Second, DO may be kinetically incorporated with a small oxygen isotope fractionation ($^{18}\varepsilon_{MnOx\text{-}O2} \approx 0$‰) and preserved in ferromanganese crusts (Mandernack et al., 1995). Lastly, DO may be kinetically incorporated in Mn oxides with a large isotope fractionation ($^{18}\varepsilon_{MnOx\text{-}O2} \approx -20$‰) and preserved in ferromanganese crusts (Mandernack et al., 1995; Sutherland et al., 2018).

First, we consider whether it is possible for an equilibrium isotope fractionation regime to play a role in the oxygen isotope composition of the ferromanganese crusts. Temperature is the main driver of variation during equilibrium oxygen isotope processes (Sharp, 2017). The $\delta^{18}O$ values of the crusts used in this study range from 5.1-11.9‰. Bottom water temperature does not vary between sites by more than a few degrees C, and the $\delta^{18}O$ value of bottom water varies by ~ 0.5‰ (Adkins et al., 2002). Since temperature and water oxygen isotope composition are essentially constant, the 6.8‰ variation in our dataset cannot be explained using equilibrium fractionation processes alone. Although there is no direct evidence of Mn oxides forming in oxygen isotope equilibrium with water, we can also evaluate whether these $\Delta'^{17}O$ values could reasonably result from equilibrium processes by looking at the inferred $\delta^{17}O$-$\delta^{18}O$ fractionation relationship between samples, or $\theta_{EQ\text{-}inferred}$. Typically, θ is used to describe a fixed triple oxygen mass relationship intrinsic to a single process at a given temperature. In this thought experiment we use $\theta_{EQ\text{-}inferred}$ and the assumption that a sample is in equilibrium with seawater, to evaluate whether the observed triple oxygen values are more consistent with a composition reflecting oxygen isotope equilibrium with seawater or some mixture of water and dissolved O_2 (Sutherland et al., 2018). Typical values of θ_{EQ} in low-temperature (0-100 °C) mineral-water oxygen isotope equilibrium vary from 0.523 to 0.525 (Bao et al., 2016; Cao and Liu, 2011). Computational studies investigating the bounds of θ between two oxygen-bearing systems (not just mineral-water pairs) have shown that θ may deviate from canonical values when $^{18}\alpha$ is low, but even still, 90% of theoretical oxygen-bearing species pairs produce θ values falling in the range 0.5285 ± 0.01 (Bao et al., 2015). In comparison, we calculate values of $\theta_{EQ\text{-}inferred}$ of 0.499 to 0.520 for the global ferromanganese crusts, with an average value of 0.513. The Mn-oxide endmember contained within these ferromanganese crusts must have a $\theta_{EQ\text{-}inferred}$ that is lower still if the other O-bearing components in the crust (e.g., Fe oxides and silicates) fall within the typical 0.523 to 0.525 range. Mn oxides with the lowest $\Delta'^{17}O$ have a $\theta_{EQ\text{-}inferred}$ of ~ 0.500, a value quite distinct from those typically observed in mineral-water equilibrium systems. Similarly low values of θ have been observed for some kinetic isotope effects related to reactive oxygen species production (derived from O_2) and some observations of respiration (Helman, 2005; Stolper et al., 2018). However, given that $\theta_{EQ\text{-}inferred}$ deviates quite significantly from typical θ_{EQ} predictions and from observations of θ_{EQ} in mineral-water systems, mineral-water oxygen isotopic equilibrium can plausibly be ruled out for these natural marine Mn-oxide phases.

Next, we consider kinetic incorporation of DO and water with very little fractionation. There is evidence for a Mn-oxide endmember that derives its oxygen from a 50:50 mixture of O_2 and H_2O with little to no oxygen isotopic fractionation with respect to each source. This has been observed in one example of bacterial Mn(II) oxidation (*Aurantimonas manganoxydans* SI85-9A1 and inferred for freshwater ferromanganese nodules form Lake Oneida (Mandernack et al., 1995)). This theoretical Mn-oxide endmember would fall on a mixing line between H_2O and O_2 (MnOx1 in Fig. 3), and could adequately explain the observed distribution of $\delta'^{18}O$ and $\Delta'^{17}O$ in the global ferromanganese crust samples (given certain constraints on the silicate endmember). While this explanation is plausible, it raises questions as to why O_2 may be subject to such a wide range of fractionation regimes during Mn oxidation. We discuss this further below (Section 3.5).

Lastly, we consider kinetic incorporation of DO with a large fractionation factor. In laboratory precipitated oxides, the oxidation of aqueous Mn(II) to Mn(III/IV) mediated by bacterial, fungal, and abiotic processes results in a large mineral-DO oxygen isotope fractionation ($^{18}\varepsilon_{MnOx\text{-}O2} = -17$ to -23‰) and a small mineral-water oxygen isotope fractionation ($^{18}\varepsilon_{MnOx\text{-}H2O} \approx 0$‰) (Mandernack et al., 1995; Sutherland et al., 2018). In these systems, approximately half of the oxygen atoms derive from each reservoir (DO and H_2O). If natural Mn oxides exhibit similar isotope fractionation factors during formation as laboratory precipitated oxides, we would expect the Mn-oxide endmember to have $\delta'^{18}O$ and $\Delta'^{17}O$ values of approximately 0–+4‰ and −0.080–−0.180‰, respectively (MnOx2 in Fig. 3, assuming starting $\delta^{18}O_{O2} = +24.5$‰, $\Delta'^{17}O_{O2} = -0.45$‰ and $\delta^{18}O_{H2O} = 0$‰, $\Delta'^{17}O_{H2O} = 0$‰, $\varepsilon_{O2} = -17$–−23‰, $\varepsilon_{O2} = 0$‰, and $\theta_{KIE} = 0.515$-0.520). This theoretical Mn-oxide endmember could explain $\delta'^{18}O$ and $\Delta'^{17}O$ values in bulk ferromanganese crusts, but would require that most silicate in the sample formed at low temperature or that θ_{KIE} be slightly higher than we assume (Fig. 3). In either case, the large fractionation framework represents most lab-based observations and can explain the $\Delta'^{17}O$ of natural ferromanganese crusts, thereby offering the most parsimonious explanation for the Mn oxide system.

Indeed, the incorporation of DO into Mn-oxide minerals under both fractionation frameworks (MnOx1 and MnOx2, Fig. 3) provides plausible explanations for the triple oxygen values and $\theta_{EQ\text{-}inferred}$ observed in the global ferromanganese crust dataset (Mandernack et al., 1995; Sutherland et al., 2018). MnOx2 offers a particularly compelling explanation as it reconciles synthetic and natural oxides. Mineral-water equilibrium does not offer a satisfactory explanation of the ferromanganese crusts $\Delta'^{17}O$. Observationally, Mn-oxide minerals precipitated by biotic and abiotic reaction mechanisms at low temperatures in circumneutral pH waters do not exchange oxygen isotopes with water (Mandernack et al., 1995). Instead, these low-temperature Mn oxides retain oxygen derived from the surrounding dissolved O_2 and water. Such a mixture of O atom sources would in fact yield values for $\theta_{EQ\text{-}inferred}$ lower than what is typically observed in mineral-water equilibrium; in fact, θ would no longer be an appropriate variable to use since our calculated θ values represent the result of an isotopic mixture and isotopic fractionation – rather than a single fractionating process.

A significant question still remains: why do Mn oxides exhibit such a significant mineral-DO oxygen isotope fractionation range? Synthetic biotic and abiotic Mn oxides are typically precipitated in systems designed to quickly oxidize a significant quantity of Mn(II), typically involving $>$ 100 μM Mn(II) and unnaturally high abundances of Mn(II)-oxidizing microbes, and likely fail to capture the complexity of Mn speciation in nature. Mn oxidation rates in nature are typically much slower than in benchtop experiments.

Further, Mn(III)-ligand complexes can comprise a significant fraction (> 80%) of the dissolved Mn pool in oxic marine environments (Oldham et al., 2017), and thus natural Mn oxides may form in large part via the one-electron oxidation of Mn(III). To our knowledge, there has been no study on the oxygen isotope effects of Mn(III)-ligand complex oxidation. The range of fractionation factors may reflect the diversity of Mn-ligand complexes and their coordination with O_2 prior to oxidation. In any case, the inferred differences in oxygen isotope fractionation between the high-fractionation and low-fractionation cases require further study to determine the conditions under which each mechanism is operative. From here we explore the utility of triple oxygen isotopes of Mn-oxide minerals and associated challenges with its realization.

3.3. Comparison to estimates of marine dissolved oxygen

We performed a pairwise linear regression of the estimated local dissolved oxygen concentration (see methods) against the other five measured parameters (Fe wt%, Mn wt%, Si wt%, $\delta^{18}O$, and $\Delta'^{17}O$, full results available in the Supplemental Material). Only two of these five parameters (Mn wt% and $\delta^{18}O$) had an R^2 greater than 0.1 when plotted against DO: Mn wt% and $\delta^{18}O$. Mn wt% and the dissolved oxygen concentration demonstrated a negative relationship with a fairly robust correlation ($R^2 = 0.72$), while bulk $\delta^{18}O$ demonstrated a rather weak positive relationship ($R^2 = 0.25$). If dissolved oxygen $\delta^{18}O$ were the primary influence on the bulk $\delta^{18}O$ of ferromanganese crusts, we would expect a negative relationship instead of the positive one we observed. One plausible explanation for this behavior is that dissolved oxygen also has significant influence on the bulk chemistry of ferromanganese crusts, most notably Mn wt%. Thus, the strong correlation between dissolved oxygen and Mn concentration may be masking some of the effect of oxygen saturation on $\delta^{18}O$ of manganese oxides in ferromanganese crusts.

To explore these correlations further and determine if our data could be further explained by relationships among the measured parameters, we performed a principal component analysis (PCA). The six principal components explain the following fraction of the total variance of the system: PC1: 43.5%, PC2: 26.0%, PC3: 13.6%, PC4: 10.6%, PC5: 5.3%, PC6: 1.0%. PC1 has high positive loading on Mn, and negative loading on all other parameters. PC2 has strong positive loadings on Si and Fe, strong negative loading on $\Delta'^{17}O$, and moderate loadings on the remaining three parameters. These two components (PC1 and PC2) account for 69.5% of the variance in the data. The long tail in the distribution of variance across the principal components highlights the complexity of this system. We hypothesize that some of this complexity arises from variability in the oxygen isotope composition of the Fe and Si endmembers, which we discuss below (Section 3.5). Additionally, variability in the oxygen isotope fractionation of Mn oxidation cannot be ruled out. Notably, the near-orthogonal nature of Mn versus Si and Fe suggests independence between Mn and the other major compositional parameters. Similarly, the strong loading of PC1 on Mn, $[O_2]$, and $\delta'^{18}O$ hint at an underlying relationship (e.g. high dissolved Mn concentrations in low oxygen settings). A full presentation of the results of this PCA are provided in the Supplementary Material.

3.4. Utility of triple oxygen isotope measurements of manganese oxides

The triple oxygen isotope signature of O_2 incorporated into ferromanganese crusts will be governed by the isotopic signature of bottom seawater and dissolved O_2, with the former having a much smaller potential dynamic range than the latter. The $\delta^{18}O$ of Mn oxides can constrain the $\delta^{18}O$ of dissolved O_2, which in turn constrains the oxygen saturation of bottom-water O_2. Assuming a 50:50 oxygen contribution from water and DO, the limit to which $\delta^{18}O$ and $\Delta'^{17}O$ may provide paleo-environmental data on dissolved O_2 is set by the fraction of the Mn-oxide endmember present in a sample. A pure Mn-oxide endmember will have ~ 50% of the isotopic dynamic range of the dissolved O_2 in which it formed, and this dynamic range will decrease proportionally with Mn content. The Mn oxides in this study ranged from 8.2 to 32.5 weight percent Mn, compared to ~ 63% for pure MnO_2. A typical ferromanganese crust from the Pacific Ocean contains approximately 19 weight percent Fe, 23 weight percent Mn, and 5 weight percent Si (Hein and Koschinsky, 2014). Approximating this assemblage as a water-free oxide mixture, approximately 50% of the oxygen in the crusts will be associated with Mn, meaning approximately 25% of mineral-bound oxygen will be from O_2.

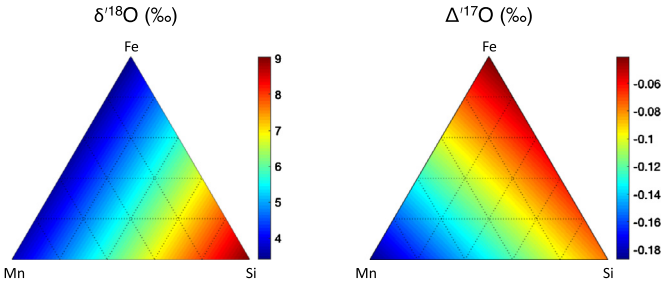

Fig. 4. Oxygen isotope ternary diagram for mixture of primary components of ferromanganese crust as MnO_2, Fe_2O_3, and SiO_2. The Mn oxide endmember is one of many possible values from MnOx2. We use hematite-water low-temperature equilibrium to estimate the oxygen isotope composition of the Fe endmember (Hayles et al., 2018). SiO_2 is calculated as a 80:20 oxygen isotopic mixture of detrital (high temperature) and authigenic (near 0 °C) SiO_2, respectively (Sharp et al., 2016). We note that the choice of endmembers in this example are non-unique, these parameters are chosen primarily to illustrate the utility of ferromanganese crust triple oxygen measurements.

To further illustrate the combination of factors that produce the $\delta^{18}O$ and $\Delta'^{17}O$ range observed in this study, we constructed a simple three endmember mixing ternary (Fig. 4). This ternary includes one possible Mn-oxide endmember for oxygen saturated bottom water (from MnOx2, Fig. 3), hematite in oxygen isotopic equilibrium with seawater at 0 °C (Hayles et al., 2018), and a mixture of SiO_2 endmembers that best fit the data in this study (20% authigenic, 80% detrital) (Sharp et al., 2016). The relatively low $\Delta'^{17}O$ of the Mn-oxide endmember produces a $\delta'^{18}O$ and $\Delta'^{17}O$ that is unique to each assemblage. In a system where the relative abundance of Mn, Fe, and Si and the isotopic composition of the Fe and Si endmembers is constrained, the Mn-oxide triple oxygen endmember, and therefore the O_2 saturation state at the time of formation, could be determined. Thus, the combination of $\delta'^{18}O$ and $\Delta'^{17}O$ of hydrogenetic ferromanganese crusts may theoretically provide a useful constraint on bottom-water dissolved oxygen over the last ~ 75 Ma, shedding light on patterns of ocean circulation, primary productivity, and respiration.

3.5. Challenges of the manganese oxide triple oxygen isotope system

Several challenges need to be addressed in the collection and measurement of $\delta'^{18}O$ and $\Delta'^{17}O$ of Mn-oxide minerals. First, the fraction of Mn-oxide oxygen derived from DO and the presumed oxygen fractionation factors need further investigation. Some evidence suggests the O_2-derived oxygen may depend on Mn oxidation state in mixed valence oxides (Sutherland et al., 2018). While these fractionation factors agree with some previous observations of synthetic and natural Mn oxides, a comprehensive explanation for the range of oxygen isotope fractionation values remains elusive. Related to this, the operative oxidation mechanism(s) in naturally occurring low-temperature Mn-oxide deposits

are still unknown. Measurements of ferromanganese crusts where the $\delta'^{18}O$ and $\Delta'^{17}O$ of modern DO and water are directly measured could provide greater insight. Phase isolation is another necessary step for triple oxygen isotope measurements of marine Mn oxides; further study of the triple oxygen isotope systematics in low-temperature Fe oxides and silicates would provide better endmember constraints. The three-dimensional compositional heterogeneity in ferromanganese crusts is another element of complexity. Geochemical phase separation has been performed on ferromanganese crusts, but none of these commonly used techniques can satisfactorily isolate the Mn-oxide endmember (Koschinsky and Halbach, 1995; Koschinsky and Hein, 2003). Leveraging internal heterogeneity among regions of similar age to calculate the Mn-oxide endmember isotope composition may be a viable approach.

4. Summary and conclusion

We investigated the bulk triple oxygen isotope signature of 13 ferromanganese crusts from throughout the global ocean for evidence of a DO signal. The range of $\delta'^{18}O$ values among deep-ocean samples collected in this study and those compiled here from previous studies suggests that the isotopic signature of water plays a significant role in determining the $\delta'^{18}O$ of Mn oxides, but water alone does not explain the full range of $\delta'^{18}O$ values in Mn oxides. Deep-ocean ferromanganese crust samples from all major ocean basins have a much lower $\Delta'^{17}O$ value than is typically observed in mineral-water equilibrium, and lower than can be explained as a mixture of Fe oxide and silicates present in the crust, providing evidence that DO is incorporated and preserved on million-year time scales in the Mn-oxide component of deep-ocean ferromanganese crusts. The combination of $\delta'^{18}O$ and $\Delta'^{17}O$ values in natural ferromanganese crusts makes it difficult to fully constrain the isotope fractionation factors associated with Mn oxidation, although lab studies suggest O_2 incorporation gives rise to a -17 to $-23‰$ oxygen isotope effect during Mn(II) oxidation, while water incorporation imparts very little oxygen isotope fractionation.

We constructed a three-component mixing model to explain the distribution of $\delta'^{18}O$ and $\Delta'^{17}O$ values in ferromanganese crusts. We propose that oxides of Mn, Fe, and Si, which make up the bulk of ferromanganese crusts, produce a bulk ferromanganese $\Delta'^{17}O$ that is the sum of their individual components. If the mineralogy and isotopic composition of the Fe and Si endmembers are well known, our model illustrates how the Mn-oxide endmember and its O_2-derived oxygen isotope composition may be calculated. While phase isolation and more thorough study of Mn(II) and Mn(III) oxidation mechanism(s) and isotope fractionation dynamics are necessary, the values we present provide a framework for future study. Despite these challenges, bulk ferromanganese crust triple oxygen isotope values provide strong evidence that hydrogenetic Mn oxides contain a previously unknown and untapped isotopic record of oceanic bottom water DO extending up to 75 Ma. Such a record promises greater insight on the saturation state of oxygen in the ocean, the balance of global productivity and respiration, and processes related to the composition of Earth's atmosphere.

Declaration of competing interest

The authors declare that they have no known competing financial interests or personal relationships that could have appeared to influence the work reported in this paper.

Acknowledgements

The authors would like to acknowledge their funding sources including NASA NESSF NNX15AR62H (KMS), NASA Exobiology grant NNX15AM04G to SDW and CMH, U.S. NSF grant #DGE-1418062 (JAGW), and NSF EAR1551226 (ZDS). This research was further supported in part by Hanse-Wissenschaftskolleg Institute of Advanced Study fellowships to CMH and SDW. The authors would also like to thank David Johnston for thoughtful and constructive feedback on an early version of this manuscript.

Appendix A. Supplementary material

Supplementary material related to this article can be found online at https://doi.org/10.1016/j.epsl.2019.116057.

References

Adkins, J.F., McIntyre, K., Schrag, D.P., 2002. The salinity, temperature, and $\delta^{18}O$ of the glacial deep ocean. Science 298, 1769–1773.

Bao, H., Cao, X., Hayles, J.A., 2015. The confines of triple oxygen isotope exponents in elemental and complex mass-dependent processes. Geochim. Cosmochim. Acta 170, 39–50. https://doi.org/10.1016/j.gca.2015.07.038.

Bao, H., Cao, X., Hayles, J.A., 2016. Triple oxygen isotopes: fundamental relationships and applications. Annu. Rev. Earth Planet. Sci. 44, 463–492. https://doi.org/10.1146/annurev-earth-060115-012340.

Bar-Matthews, M., Matthews, A., 1990. Chemical and stable isotope fractionation in manganese oxide-phosphorite mineralization, Timna Valley, Israel. Geol. Mag. 127, 1–12.

Barkan, E., Luz, B., 2005. High precision measurements of O-17/O-16 and O-18/O-16 ratios in H_2O. Rapid Commun. Mass Spectrom. 19, 3737–3742. https://doi.org/10.1002/rcm.2250.

Basu, S., Stuart, F.M., Klemm, V., Korschinek, G., Knie, K., Hein, J.R., 2006. Helium isotopes in ferromanganese crusts from the central Pacific Ocean. Geochim. Cosmochim. Acta 70, 3996–4006.

Bender, M., Sowers, T., Labeyrie, L., 1994. The Dole Effect and its variations during the last 130,000 years as measured in the Vostok Ice Core. Glob. Biogeochem. Cycles 8, 363–376. https://doi.org/10.1029/94gb00724.

Blunier, T., Barnett, B., Bender, M.L., Hendricks, M.B., 2002. Biological oxygen productivity during the last 60,000 years from triple oxygen isotope measurements 16.

Cao, X., Bao, H., 2013. Dynamic model constraints on oxygen-17 depletion in atmospheric O_2 after a snowball Earth. Proc. Natl. Acad. Sci. 110. https://doi.org/10.1073/pnas.1302972110.

Cao, X., Liu, Y., 2011. Equilibrium mass-dependent fractionation relationships for triple oxygen isotopes. Geochim. Cosmochim. Acta 75, 7435–7445. https://doi.org/10.1016/j.gca.2011.09.048.

Chyi, M.S., Crerar, D.A., Carlson, R.W., Stallard, R.F., 1984. Hydrothermal Mn-deposits of the Franciscan Assemblage, II. Isotope and trace element geochemistry, and implications for hydrothermal convection at spreading centers 71, 31–45.

Clayton, R.N., Mayeda, T.K., 1996. Oxygen isotope studies of achondrites. Geochim. Cosmochim. Acta 60, 1999–2017.

Clayton, R.N., Mayeda, T.K., Olsen, E.J., Prinz, M., 1983. Oxygen isotope relationships in iron meteorites. Earth Planet. Sci. Lett. 65, 229–232.

Crockford, P.W., Hayles, J.A., Bao, H., Planavsky, N.J., Bekker, A., Fralick, P.W., Halverson, G.P., Bui, T.H., Peng, Y., Wing, B.A., 2018. Triple oxygen isotope evidence for limited mid-Proterozoic primary productivity. Nature 559, 613–616. https://doi.org/10.1038/s41586-018-0349-y.

Dymond, J., Corliss, J.B., Heath, G.R., Field, C.W., Dasch, E.J., Veeh, H.H., 1973. Origin of metalliferous sediments from the Pacific Ocean.

Flanagan, F.J., Gottfried, D., 1980. USGS rock standards; III, manganese-nodule reference samples USGS-Nod-A-1 and USGS-Nod-P-1.

Frank, M., O'Nions, R.K., Hein, J.R., Banakar, V.K., 1999. 60 Myr records of major elements and Pb-Nd isotopes from hydrogenous ferromanganese crusts: reconstruction of seawater paleochemistry. Geochim. Cosmochim. Acta 63, 1689–1708. https://doi.org/10.1016/s0016-7037(99)00079-4.

Garcia, H.E., Weathers, K., Paver, C.R., Smolyar, I., Boyer, T.P., Locarnini, R.A., Zweng, M.M., Mishonov, A.V., Baranova, O.K., Seidov, D., Reagan, J.R., 2018. World Ocean Atlas 2018, vol. 3, Dissolved Oxygen, Apparent Oxygen Utilization, and Oxygen Saturation.

Gehler, A., Tütken, T., Pack, A., 2011. Triple oxygen isotope analysis of bioapatite as tracer for diagenetic alteration of bones and teeth. Palaeogeogr. Palaeoclimatol. Palaeoecol. 310, 84–91. https://doi.org/10.1002/cctc.201300971.

Halbach, P., Kriete, C., Prause, B., Puteanus, D., 1989. Mechanisms to explain the platinum concentration in ferromanganese seamount crusts. Chem. Geol. 76, 95–106.

Hayles, J., Gao, C., Cao, X., Liu, Y., Bao, H., 2018. Theoretical calibration of the triple oxygen isotope thermometer. Geochim. Cosmochim. Acta 235, 237–245. https://doi.org/10.1016/j.gca.2018.05.032.

Hein, J.R., Koschinsky, A., 2014. Deep-ocean ferromanganese crusts and nodules. In: The Treatise on Geochemistry.

Helman, Y., 2005. Fractionation of the three stable oxygen isotopes by oxygen-producing and oxygen-consuming reactions in photosynthetic organisms. Plant Physiol. 138, 2292–2298. https://doi.org/10.1104/pp.105.063768.

Hoffmann, G., Cuntz, M., Weber, C., Ciais, P., Friedlingstein, P., Heimann, M., Jouzel, J., Maier-Reimer, E., Seibt, U., Six, K., 2004. A model of the Earth's Dole effect. Glob. Biogeochem. Cycles 18, 1–15. https://doi.org/10.1029/2003GB002059.

Hulston, J.R., Thode, H.G., 1965. Variations in the S33, S34, and S36 contents of meteorites and their relation to chemical and nuclear effects. J. Geophys. Res. 70, 3475–3484.

Koschinsky, A., Halbach, P., 1995. Sequential leaching of marine ferromanganese precipitates: genetic implications 59, 5113–5132.

Koschinsky, A., Hein, J.R., 2003. Uptake of elements from seawater by ferromanganese crusts: solid-phase associations and seawater speciation. Mar. Geol. 198, 331–351. https://doi.org/10.1016/s0025-3227(03)00122-1.

Kroopnick, P., 1980. Isotopic fractionations during oxygen consumption and carbonate dissolution within the North-Atlantic Deep-Water. Earth Planet. Sci. Lett. 49, 485–498. https://doi.org/10.1016/0012-821x(80)90089-8.

Learman, D.R., Voelker, B.M., Vazquez-Rodriguez, A.I., Hansel, C.M., 2011. Formation of manganese oxides by bacterially generated superoxide. Nat. Geosci. 4, 95–98. https://doi.org/10.1038/ngeo1055.

Levin, N.E., Raub, T.D., Dauphas, N., Eiler, J.M., 2014. Triple oxygen isotope variations in sedimentary rocks. Geochim. Cosmochim. Acta 139, 173–189. https://doi.org/10.1016/j.gca.2014.04.034.

Levine, N.M., Bender, M.L., Doney, S.C., 2009. The $\delta^{18}O$ of dissolved O_2 as a tracer of mixing and respiration in the mesopelagic ocean. Glob. Biogeochem. Cycles 23, 1–12. https://doi.org/10.1029/2007GB003162.

Luther, G.W., 2010. The role of one- and two-electron transfer reactions in forming thermodynamically unstable intermediates as barriers in multi-electron redox reactions. Aquat. Geochem. 16, 395–420. https://doi.org/10.1007/s10498-009-9082-3.

Luz, B., Barkan, E., Bender, M.L., Thiemens, M.H., Boering, K.A., 1999. Triple-isotope composition of atmospheric oxygen as a tracer of biosphere productivity. Nature, 547–550. https://doi.org/10.1038/22987.

Mandernack, K.W., Fogel, M.L., Tebo, B.M., Usui, A., 1995. Oxygen isotope analyses of chemically and microbially produced manganese oxides and manganates. Geochim. Cosmochim. Acta 59, 4409–4425. https://doi.org/10.1016/0016-7037(95)00299-f.

Menicucci, A.J., Matthews, J.A., Spero, H.J., 2013. Oxygen isotope analyses of biogenic opal and quartz using a novel microfluorination technique. Rapid Commun. Mass Spectrom. 27, 1873–1881. https://doi.org/10.1002/rcm.6642.

Miller, M.F., 2002. Isotopic fractionation and the quantification of O-17 anomalies in the oxygen three-isotope system: an appraisal and geochemical significance. Geochim. Cosmochim. Acta 66, 1881–1889. https://doi.org/10.1016/s0016-7037(02)00832-3.

Oldham, E., Mucci, A., Tebo, B.M., Luther, G.W., 2017. Soluble Mn(III)–L complexes are abundant in oxygenated waters and stabilized by humic ligands. Geochim. Cosmochim. Acta 199, 238–246. https://doi.org/10.1016/j.gca.2016.11.043.

Pack, A., Höweling, A., Hezel, D.C., Stefanak, M.T., Beck, A.K., Peters, S.T.M., Sengupta, S., Herwartz, D., Folco, L., 2017. Tracing the oxygen isotope composition of the upper Earth's atmosphere using cosmic spherules. Nat. Commun. 8, 1–7. https://doi.org/10.1038/ncomms15702.

Sengupta, S., 2016. Triple oxygen isotopes of cherts: implications for the $\delta^{18}O$ and temperatures of early oceans.

Sharp, Z.D., 1990. A laser-based microanalytical method for the in situ determination of oxygen isotope ratios of silicates and oxides. Geochim. Cosmochim. Acta 54, 1353–1357.

Sharp, Z.D., 2017. Principles of stable isotope geochemistry.

Sharp, Z.D., Gibbons, J.A., Maltsev, O., Atudorei, V., Pack, A., Sengupta, S., Shock, E.L., Knauth, L.P., 2016. A calibration of the triple oxygen isotope fractionation in the SiO_2–H_2O system and applications to natural samples. Geochim. Cosmochim. Acta 186, 105–119. https://doi.org/10.1016/j.gca.2016.04.047.

Sharp, Z.D., Wostbrock, J.A.G., Pack, A., 2018. Mass-dependent triple oxygen isotope variations in terrestrial materials. Geochem. Perspect. Lett., 27–31. https://doi.org/10.7185/geochemlet.1815.

Stolper, D.A., Fischer, W.W., Bender, M.L., 2018. Effects of temperature and carbon source on the isotopic fractionations associated with O_2 respiration for 17O/16O and 18O/16O ratios in E. coli. Geochim. Cosmochim. Acta 240, 152–172. https://doi.org/10.1016/j.gca.2018.07.039.

Sutherland, K.M., Wankel, S.D., Hansel, C.M., 2018. Oxygen isotope analysis of bacterial and fungal manganese oxidation. Geobiology. https://doi.org/10.1111/gbi.12288.

Tebo, B.M., Johnson, H.A., McCarthy, J.K., Templeton, A.S., 2005. Geomicrobiology of manganese(II) oxidation. Trends Microbiol. 13, 421–428. https://doi.org/10.1016/j.tim.2005.07.009.

Thiemens, M.H., 2006. History and applications of mass-independent isotope effects. Annu. Rev. Earth Planet. Sci. 34, 217–262. https://doi.org/10.1146/annurev.earth.34.031405.125026.

Thiemens, M.H., Heidenreich, J.E., 1983. The mass-independent fractionation of oxygen: a novel isotope effect and its possible cosmochemical implications 219, 1073–1075.

Uramoto, G.I., Morono, Y., Tomioka, N., Wakaki, S., Nakada, R., Wagai, R., Uesugi, K., Takeuchi, A., Hoshino, M., Suzuki, Y., Shiraishi, F., Mitsunobu, S., Suga, H., Takeichi, Y., Takahashi, Y., Inagaki, F., 2019. Significant contribution of subseafloor microparticles to the global manganese budget. Nat. Commun. 10, 1–10. https://doi.org/10.1038/s41467-019-08347-2.

Wostbrock, J.A.G., Cano, E., Sharp, Z.D., 2020. An internally consistent triple oxygen isotope calibration of standards for silicates, carbonates and air relative to VSMOW2 and SLAP2. Chem. Geol. 533, 119432.

Yeh, H.-W., Hein, J.R., Koski, R.A., 1985. Stable-Isotope Study of Volcanogenic- and Sedimentary-Manganese Deposits. Open File Rep. 85-662. United States Dep. Inter. Geol. Surv.

Zachos, J., Pagani, M., Sloan, L., Thomas, E., Billups, K., 2001. Trends, rhythms, and aberrations in global climate 65 Ma to present. Science 292, 686–693.